The 8th European Congress on Computational Methods in Applied Sciences and Engineering
ECCOMAS Congress 2022
5 – 9 June 2022, Oslo, Norway

THERMAL AND STRUCTURAL MODELLING OF THERMOSET COMPOSITE REPAIRS TOWARDS OPTIMIZATION OF THE CURE CYCLE FOR MINIMUM DISTORTION

TIM P.A. KOENIS*, NIELS VAN HOORN* AND MARIE MOGHADASI*

* Royal Netherlands Aerospace Centre (NLR)
Anthony Fokkerweg 2, 1059 CM Amsterdam, Netherlands
e-mail: Tim.Koenis@nlr.nl, www.nlr.org

Key words: Numerical Methods, Composite Scarf Repair, Virtual Manufacturing

Abstract. During manufacturing of composite materials residual stresses can result in distortion of the final part. This distortion is even more critical when building on existing parts, such as for a repair, as the added material has to conform to the original structure. To predict this distortion due to curing of thermoset carbon-matrix composite repairs, a numerical modelling method is employed. The temperature cycle applied for the cure of thermoset composites can significantly influence the amount of residual stress and resulting deformation after manufacturing. Therefore, a method is devised to parametrise and subsequently tune this temperature cycle for minimum distortion after manufacturing. Numerical tests with the optimised temperature cycle resulted in a 36% reduction in process induced strain for a repair of a flat laminate plate. The same methodology is applied to a wing box consisting of two composite skins connected by two C-spars where a scarf repair is applied in the skin. The repair patch is locally heated by a heating blanket to cure the repair patch. A subsequent thermal-mechanical model is used to investigate the amount of residual stress and strain after cure and the influence of underlying structural elements on the repair. The developed framework can support the patch fabrication with accurate design and analysis for repairs with minimum distortion. Which in turn will result in development of cost-effective composite repairs.

1 INTRODUCTION

The use of Carbon Fibre Reinforced Polymer (CFRP) materials in aircraft structures is increasing significantly and advanced manufacturing capabilities are required to accomplish efficient and effective use of these materials. The production process can be optimised by numerical process simulation (i.e., virtual manufacturing). For instance, to minimise the residual stresses to ensure a first-time-right composite part.

Process simulation is a topic that has been extensively researched. Specifically on the composite curing process numerous PhD researches have been conducted. Johnston [1] investigated process-induced deformation for autoclave processing and defined the CHILE approach. Wijskamp, Svanberg, and Garstka [2, 3, 4] investigated process induced distortions to allow for high-precision composite manufacturing. Similarly, Nielson focussed on larger parts for wind turbines [5]. Their approaches show similarities and these methods have been implemented by authors to assess the sensitivities of input parameters [6, 7]. Their approaches have mainly been applied to generic composite parts. However, it has become imperative to also focus on structural repairs of composite parts. A successful repair can prevent replacement of a part and reduce the cost and downtime. Beside structural assessment of composite repairs [8, 9] the literature on process simulation of composite repairs is limited [10, 11]. Additionally, as composites in aerospace become more advanced, obtaining sufficient material data for accurate modelling can be a challenging and expensive process [12]. One example are Bismaleimide (BMI) resins that are used for high temperature applications [13, 14].

The goal of this paper is to predict residual stresses due to curing for repair applications with a HTA40/RM3000 BMI material. In Section 2, the modelling methods and implementations are discussed. In Section 3, the developed cure model is employed to optimize a two hold-stage cure cycle for minimal formation of residual stress. This optimized cure cycle is first applied to a repair of a flat laminate plate. Finally, in Section 4 this methodology will be applied to model a scarf repair of a generic wing box, modelling laminate skins and aluminium substructures.

2 CURE MODELLING METHOD

In this study, the resin cure is modelled using a calibrated cure kinetics model in combination with the Cure Hardening Instantaneously Linear Elastic (CHILE) model. This is extensively discussed in previous research, and therefore will only be shortly discussed in this paper [12]. The initial implementation of the model is performed in a MATLAB routine to evaluate the degree of cure and developed strains and stresses in a single point.

2.1 Modelling method

To characterize the RM3000 resin isothermal and dynamic Differential Scanning Calorimeter (DSC) measurements have been performed using a TA instruments Q2000 DSC equipped with a Tzero pan. To describe the cure kinetics of the RM3000 resin system, the autocatalytic Kamal-Sourour model was found to be adequate. The Kamal-Sourour model describes the cure rate as

$$\frac{d\alpha}{dt} = (k_1 + k_2\alpha^m)(1-\alpha)^n \tag{1}$$

with m and n as material constants, α the degree of cure, and k_1 and k_2 as rate constants defined as

$$k_i = A_i e^{\left(\frac{-E_i}{R\,T}\right)}\, with\ i = 1{,}2 \tag{2}$$

with A_i the pre-exponential constant, E_i the activation energy, R the universal gas constant, and T the absolute temperature [13]. A non-linear regression method in MATLAB fits the Kamal-Sourour model parameters, A_i, E_i, m and n to the obtained experimental DSC data [12]. The glass transition temperature is defined by the Di Benedetto relation as a function of the degree of cure [14].

$$T_g(\alpha) = T_{g0} + \frac{\lambda\alpha\left(T_{g\infty} - T_{g0}\right)}{1-\alpha(1-\lambda)} \tag{3}$$

Here T_{g0} and $T_{g\infty}$ are the glass transition temperatures at zero degree of cure and one degree of cure respectively and λ a material dependent fitting parameter. These parameters have been calibrated to glass transition temperature measurements using the Optimold cure sensor by Syntesites demonstrated in Pantelelis et al. [15]. The T_g measurements for this calibration were obtained during the cure cycle of a HTA40-RM3000 laminate.

To obtain the degree of cure at gelation (α_{gel}), isothermal DSC experiments have been performed at temperatures of 200, 220, and 240 °C. The method proposed by Gao et al. is employed to determine the degree of cure at gelation from the isothermal DSC measurements [16]. Table 1 displays the Kamal-Sourour parameters as well as the Di Benedetto parameters and degree of cure at gelation as used in this study.

Table 1: Parameters used to characterise the RM3000 BMI resin

Kamal-Sourour parameter	Value	Resin Parameter	Value
A_1 [s^{-1}]	1,605,520	$T_{g\infty}$ [°C^{-1}]	233
E_1 [J mol^{-1}]	85,506	T_{g0} [°C^{-1}]	15.7
A_2 [s^{-1}]	7,299,464	λ [-]	0.75
E_2 [J mol^{-1}]	85,317	α_{gel} [-]	0.77
n [-]	1.7695		
m [-]	3.3057		

During the curing process the resin transforms from a liquid, to a rubbery like material, and finally to a solid glassy phase. For a correct representation of the resin state an accurate constitutive model is needed. Full viscoelastic models give the closest approximation but require extensive material characterisation [4]. A good alternative is the Cure-Hardening Instantaneously Linear Elastic (CHILE) model by Johnston et al. [1, 17]. This model has been implemented and calibrated for the RM3000 resin in previous work of the authors [12].

The cure dependent resin properties and the fibre properties are homogenised using the Composite Cylinder Assemblage (CCA) model [18, 19] to obtain UD ply properties. To obtain the twill weave ply properties required for the repair the classical laminate theory is employed as demonstrated by Hoorn et al. [20]. To obtain the twill weave homogenized coefficient of thermal expansion (CTE) and chemical shrinkage (CCS) a more elaborate method is employed in the form of the Mosaic model of Ishikawa and Chou [21]. As a result, the full three-dimensional twill weave ply properties can be described as a function of T_g. The complete modelling method is implemented in the EXPAN and USDFLD subroutines in Abaqus, which has been validated for the fully characterized AS4/8852 laminates in previously published research [12].

3 CURE OPTIMIZATION

A strong advantage of virtual manufacturing simulations is the low cost of process optimization, as no extensive trial and error experimentation is required. To demonstrate some possibilities with the developed cure models, an investigation is performed where the cure models are employed to minimize the amount of deformation occurring due to curing.

3.1 Optimization method

A two stage hold cure cycle is parametrized to systematically vary the cure cycle and easily evaluate different cure cycles. Figure 1 displays the original two hold cure cycle used for HTA40/RM3000 laminates, where the temperature profile can be fully described using nine parameters. From these parameters, T1 and T4 are fixed, as T1 is the injection temperature and T4 the ambient temperature.

Of the nine variables describing the cure cycle, seven are varied in the optimization. The dwell times (d_1 and d_2) and heat-up rates (r_1, r_2 and r_3) range from 10-200% of the original value. The upper and lower bound of the first dwell temperature (T_2) are 135 and 155 °C and of the second dwell temperature (T_3) 185 and 200 °C. Using the Saltelli sampling sequence combinations for the seven input parameters (D) are generated as input [22]. Per parameter an interval (N) of 10,000 is used, resulting in $2N(D+1) = 160{,}000$ sampled cure cycles.

Due to the large number of variables, an analysis with the Abaqus implementation will not be possible within an acceptable time frame. Therefore, the MATLAB implementation is chosen for initial optimization of the cure cycle. As only a single point is evaluated, no computationally expensive Finite Element Analysis (FEA) is required. This reduces the single analysis from 15 minutes to 0.05 seconds, making it possible to evaluate all cure cycles in just over two hours. Per evaluated cure cycle, the process induced thermal and chemical strain, the degree of cure, and total manufacturing time is determined. Besides minimizing for process induced strain, the degree of cure after manufacturing should be sufficiently high. Furthermore, the total manufacturing should not be extremely long and cumbersome to implement in practice.

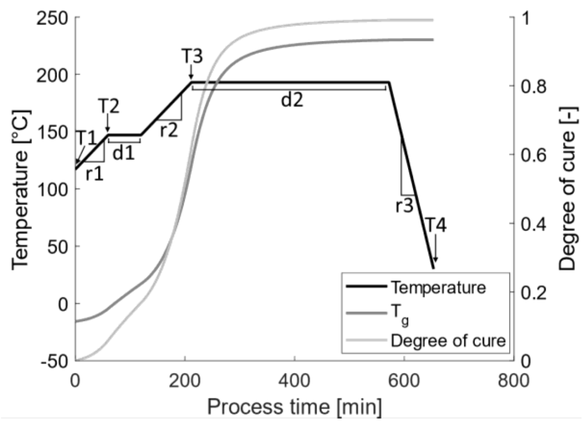

Figure 1: The nine parameters that describe the original cure cycle applied to the composite repairs.

3.2 Optimal cure cycle

When the MATLAB routine is finished the results are analysed using the Sobol method to obtain the sensitivity of the degree of cure and total strain to the 7 parameters describing the cure cycle [23]. These sensitivities are used to gain insight in the process. An overview of the sensitivities is displayed in Figure 2. It is observed that the degree of cure is largely influenced by the duration of the second dwell (T_3). However, the process induced deformation is mainly influenced by the duration of the first dwell combined with effects of other parameters.

Subsequently, the results of the analysis can be employed to extract an optimal cure cycle. From each of the 160,000 evaluated cure cycles the total strain after manufacturing is known. By selecting the cure cycle which results in the lowest strain, a near optimum cure cycle within the given bounds is found. A feasible cure cycle is ensured by constraining the final degree of cure and total manufacturing time. Only cure cycles resulting in a degree of cure larger than

95% and with a manufacturing time less than 16 hours are included. Furthermore, cure cycles with temperature ramps larger than 2 °C/min are excluded as these ramps might not be feasible with the current cure set-up.

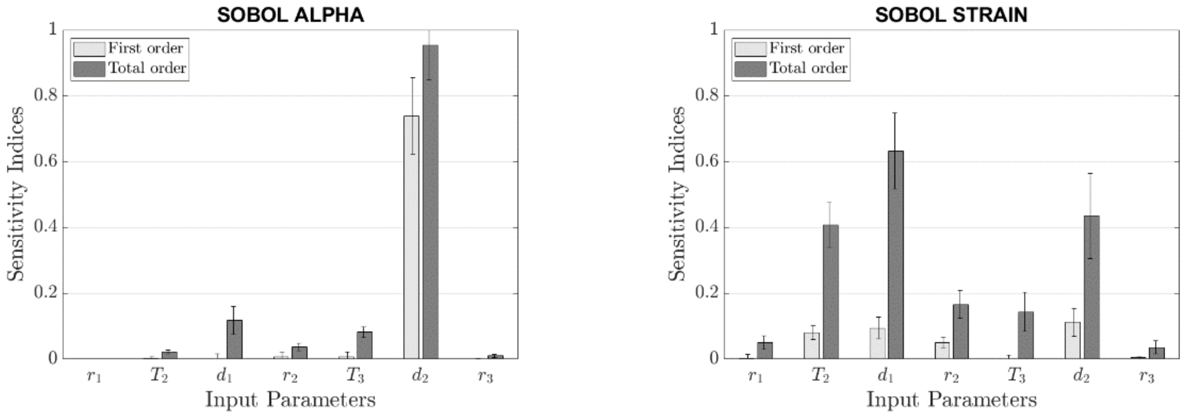

(a) **(b)**

Figure 2: First order Sobol indices and total-effect indices indicating the sensitivity of the seven parameters describing the cure cycle for (a) the degree of cure and (b) the process induced strain.

The cure cycle resulting in the least strain after manufacturing is displayed in **Figure 3**. The most remarkable feature of this cure cycle is the lengthy first dwell, and relatively short second dwell. Analysis of the 50 cure cycles with the lowest strain shows that the best cure cycles reach the gelation point ($\alpha = 0.77$) moments before the end of the first dwell. As soon as the gelation point is reached strains begin to develop, see **Figure 3** (a) and (b). By placing the second temperature ramp directly after gelation the chemical shrinkage mostly cancels out the thermal expansion. The optimal two hold stage cure cycle can reduce the total developed strain by 19%. It should be noted that these results are influenced by the accuracy of the resin characterisation. In case the degree of cure is predicted inaccurately, the modelled gelation point might shift. This would reduce the effectiveness of the optimized cure cycle.

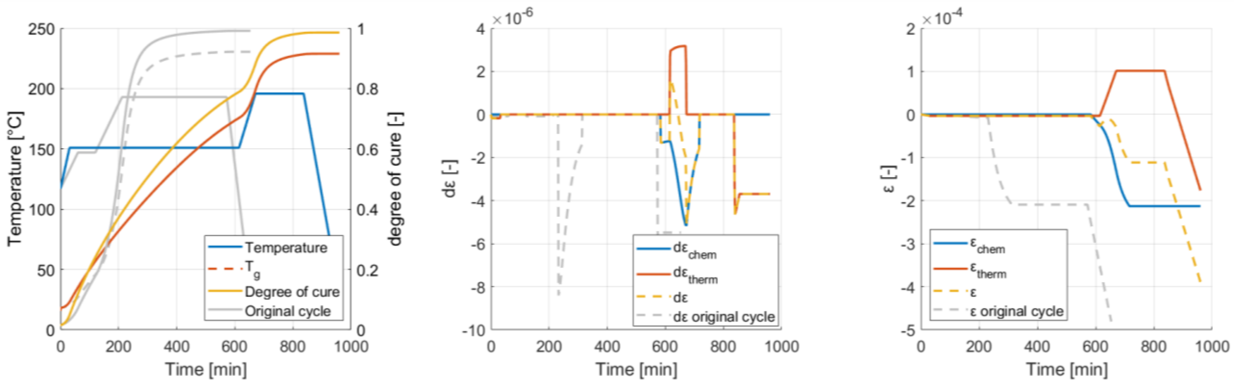

(a) **(b)** **(c)**

Figure 3: Optimal cure cycle determined for the 160,000 analyzed cycles showing (a) the temperature profile, degree of cure and Tg evolution, (b) the incremental strains and (c) the total strains.

3.3 Application of the optimized cure cycle

Abaqus is used to verify that the optimal cure cycle reduces the amount of residual stress in laminate repairs. A FEA of a 2.2 mm thick scarf repair in a 300 x 300 x 4.4 mm laminate using the optimized cure cycle is performed. The parent material consists of fully cured CYCOM 5250-4 prepreg material where the outline of the scarf repair is removed. The scarf repair consists of 12 layers of twill weave HTA-40 plies with an initial ply size of 33 x 300 mm expanding with a ratio of 1/20 to a width of 121 x 300 mm, see Figure 4 (a). Finally, four additional layers are added extending above the parent material, overlapping the repair where the width increases from 131 to 171 mm. The parent material has a layup of $[45,0,-45,90]_{4s}$. The plies of the repair patch are oriented with the same layup as the parent material.

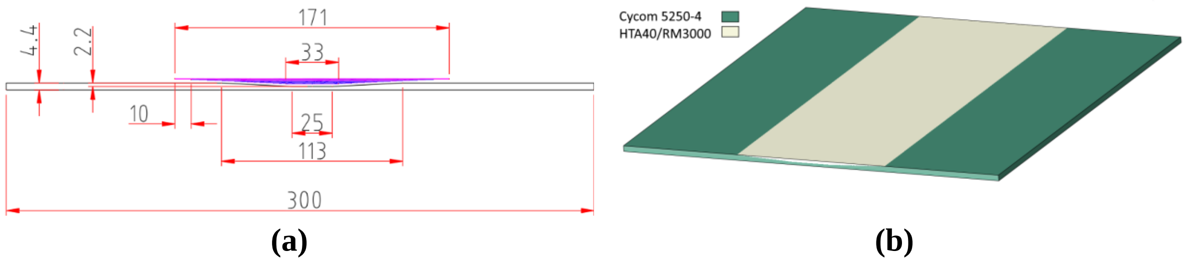

Figure 4. (a) schematic view of the scarf repair including measurements of the geometry removed from the parent material as well as the geometry of the scarf repair patch and (b) the simplified numerical model obtained to represent the scarf repair.

The scarf geometry is simplified for the numerical modelling approach. The layer thickness of the repair is assumed equal to the layer thickness of the parent material. Therefore, the 16 plies of the scarf repair conform with the parent material. Furthermore, a perfect bond between the repair and the parent material is assumed. The laminate is meshed using quadratic hex elements of 10 x 10 mm and a 1 element per ply thickness. The numerical representation of the scarf repair is displayed in Figure 4 (b).

Table 2: Properties of the CYCOM 5250-4 parent material [24] and the repair resin and fibre parameters [12].

Parent ply properties	**Cycom 5250-4**	**Repair resin properties**	**RM3000**	**Repair fibre properties**	**HTA40**
ρ [kg/m^3]	1556	ρ_m [kg/m^3]	1 250	ρ_f [kg/m^3]	1 760
E_{11}[GPa]	162	$E_{m,G}$ [MPa]	3.2e3	$E_{f,11}$ [MPa]	238e3
E_{22}, E_{33}[GPa]	9.51	$E_{m,R}$ [MPa]	3.52	$E_{f,22,33}$ [MPa]	15e3
ν_{12}, ν_{13}, ν_{23}[-]	0.32	$\nu_{m,G}$ [-]	0.365	$\nu_{f,12,13}$ [-]	0.3
G_{12}, G_{13}[GPa]	5.9	$\nu_{m,R}$ [-]	0. 4996	$\nu_{f,23}$ [-]	0.3
G_{23}[GPa]	3.3	$G_{m,G}$ [MPa]	1.17e3	$G_{f,12,13}$ [MPa]	25
CTE_{11}[°C^{-1}]	-1.32 E-6	$G_{m,R}$ [MPa]	1.17	$G_{f,23}$ [MPa]	7
CTE_{22}[°C^{-1}]	30.06 E-6	$CTE_{m,G}$ [°C^{-1}]	4.028E-5	$CTE_{f,11}$[°C^{-1}]	-1E-7
CTE_{33}[°C^{-1}]	0	$CTE_{m,R}$ [°C^{-1}]	3*$CTE_{m,G}$	$CTE_{f,22}$[°C^{-1}]	5.012E-7
		CCS [-]	-0.03252		

During the cure cycle, the a homogenous temperature is assumed in the thin laminate [12]. Only the scarf repair experiences a change in degree of cure, as the parent material is already cured. The bottom surface of the laminate is pinned, allowing no translations in this surface. After cure, the laminate is released, and fixed at the corners to avoid rigid body motions. The material properties used for the parent and repair materials are displayed in Table 2.

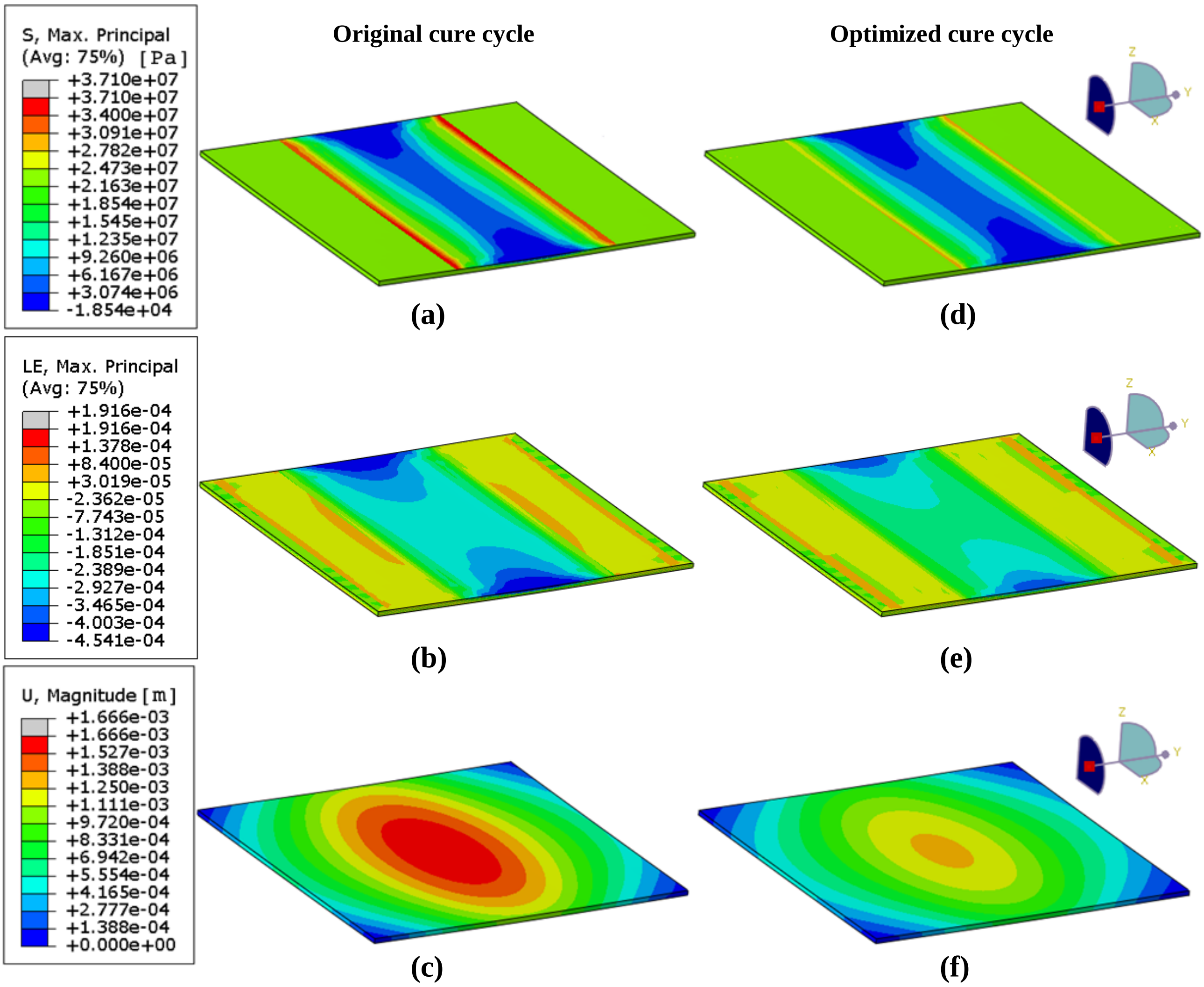

Figure 5: Results of the cure simulation on the twill weave HTA40 RM3000 scarf repair in a 300x300 mm CYCOM-5250-4 laminate with (a-c) the original cure cycle and (b-f) the optimized cure cycle. (a) and (d) show the residual max principal stress, (b) and (e) the logarithmic max principal strain and (c) and (f) the absolute deformation.

Both the original and the optimized cure cycle are applied in the Abaqus model of the scarf repair. The resulting deformation and logarithmic max principal strain and stresses are displayed in Figure 5 (a-f) for both cure cycles. The residual stresses developed during the original cure cycle are significant but not excessive. However, the residual stress is located at the bond between the repair and the parent material, which is detrimental for the adherence of the repair to the parent material. The optimized cure cycle shows a strong reduction in residual tension stress, especially at the bond region between repair and parent material where the peak stress is reduced by 18%. Similarly, the principal strains after curing show a reduction of 36% in peak strain for the optimised cure cycle. As is observed from the deformation results the effects of the optimized cure results in a repair with 23% less deformation.

4 WINGBOX REPAIR

Finally the numerical framework for repair simulation is applied to a repair of a generic wing box. The wing box consists of two 500 x 800 x 4.256 mm composite skins of UD-CYCOM material fixed by 800 x 85 x 27.5 mm aluminium C-spars. The connection between the 2.5 mm thick C-spars and the skins is made by 26 rivets per connecting surface. At the centre of the top skin, material is removed to accommodate a scarf repair to half the depth of the parent material with a ratio of 1/20 and an outer diameter of 153 mm. This material is replaced by uncured repair plies consisting of twill weave HTA-40 RM3000 plies. The parent material has a layup of $[45,0,-45,90]_{4,s}$. The plies of the repair patch are oriented with the same layup as the parent material.

4.1 Model setup

Figure 6 displays the finite element model of the wing box including the scarf repair. The aluminium spars and the elements in the vicinity of the repair patch are modelled using quadratic hexahedral elements. To limit the computational cost of the model the bottom skin and the elements in the upper skin that are at sufficient distance from the repair patch are meshed with linear hexahedral elements. The plies in the repaired laminate are meshed individually with 1 element over the ply thickness.

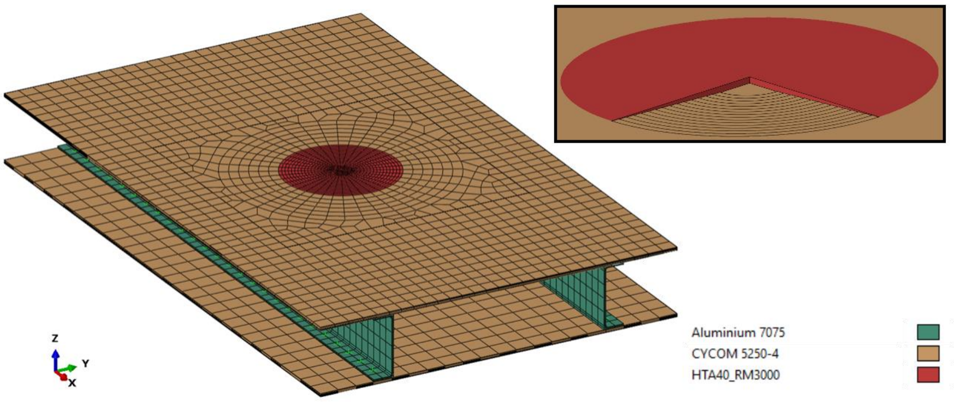

Figure 6: Finite element model of the wing box repair, displaying the aluminium spars, the CYCOM 5250-4 skins and the HTA40 RM3000 repair patch with a close up of ¾ of the patch showing the scarf angle.

In contrast with the simple 1D scarf repair, the wing box repair is heated locally by the heating blanket resulting in a inhomogeneous temperature distribution. To obtain this temperature distribution a thermal analysis is performed. Figure 7 shows a basic repair set-up for the generic wing box as modelled in this section. In the thermal simulation heat is applied to the top skin over a diameter of 300 mm centred around the repair patch. As the heating blanket is temperature controlled, it is assumed that the area below the blanket follows the applied temperature cycle. Isolated boundaries are used for the rest of the top skin, as it is isolated by breather material and the vacuum bag, and the edges of the bottom skin resting on the wooden blocks. Convective and radiative boundary conditions are applied to all other outer surfaces of the wing box based on Moser [25]. Furthermore, open cavity radiation is defined at the inside of the wing box assuming an emissivity of 0.95 for the laminates and 0.1 for the aluminium spars.

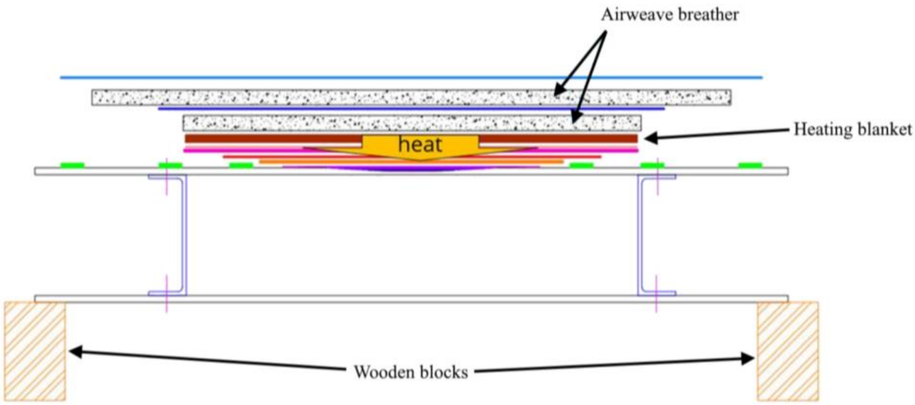

Figure 7: The repair setup for repair of the modelled wing box

The temperature profile obtained in the thermal analysis is given as load in the structural analysis. Furthermore, this temperature is used in the cure kinetics model to determine the cure induced strains and residual stresses. As the wing box is free to deform, boundary conditions are only applied to three corners of the bottom skin to prevent rigid body motions. The rivet connections between the composite skins and the aluminium spars are modelled by fixing the elements in the spars and the skins located in a small radius around the rivet to each other.

4.2 Results and discussion

Figure 8 displays the max principal stress and max principal strain in the generic wing box after cure. Similarly to the repair in the simple laminate, the peak residual stresses and strains occur at the interface between the repair and the parent material. It is observed that the peak stresses are almost double the peak stresses in the simple laminate. It is suspected that his is due to a stronger constraint on the repaired material, as the repaired skin is fixed by the aluminium spars. The effect of the optimized cure cycle on the residual stress remains evident, where the peak tension stress is reduced by 18.6%. Similarly, the peak principal strain is reduced by 22.7% when applying the optimized cure cycle. It is also observed that due to the strains in the repair patch, the connections between the skins and the spars are loaded, resulting in additional stresses in the rivet connections.

As stated before, the reduction in process induced stresses and strains strongly depends on the accuracy of the cure modelling, the used material parameters as well as the predicted temperatures. A large contributing factor in the strain reduction is the moment of gelation. As observed during the optimization of the cure cycle, it is preferred to cross the gelation point before the second temperature ramp to limit process induced strains. In the numerical simulations, this moment is strongly dependent on the cure kinetics, degree of cure at gelation and predicted temperatures, where small changes in these parameters can significantly limit the effect of the optimized cure cycle. However, even without accurate resin characterization and temperature prediction insights gained in this study could still be valuable. If during the actual curing of a repair the gelation point can be detected, this could be used as a trigger to ramp to the second dwell temperature, effectively reproducing the working principles behind the optimized cure cycle.

Besides the cure characterization, the obtained results are also strongly dependent on the used ply properties, such as the chemical shrinkage and thermal expansion coefficients. Full characterization of the materials can be a laborious and expensive process which can strongly limit the accuracy of the virtual manufacturing of composite materials. Therefore, further experimental validation of the employed models using the generic wing box is required.

5 CONCLUSIONS

- Cure kinetic modelling combined with parametrization of the cure cycle can quickly give insights in the effects of different cure cycles, and how to perform an optimal cure cycle to strongly reduce process induced residual stresses
- The optimal cure cycle was first tested numerically on a simple scarf repair showing a significant reduction in the process induced strain of up to 36%.
- Finally, the framework is successfully applied to a model representing a generic wing box, showing the effectiveness of the optimized cure cycle while taking into account the underlying structures.
- It is shown that this framework with optimisation of the cure cycle can support the patch fabrication with accurate design and analysis for repairs with minimum distortion. However, further experimental validation of the modelling approach is required.

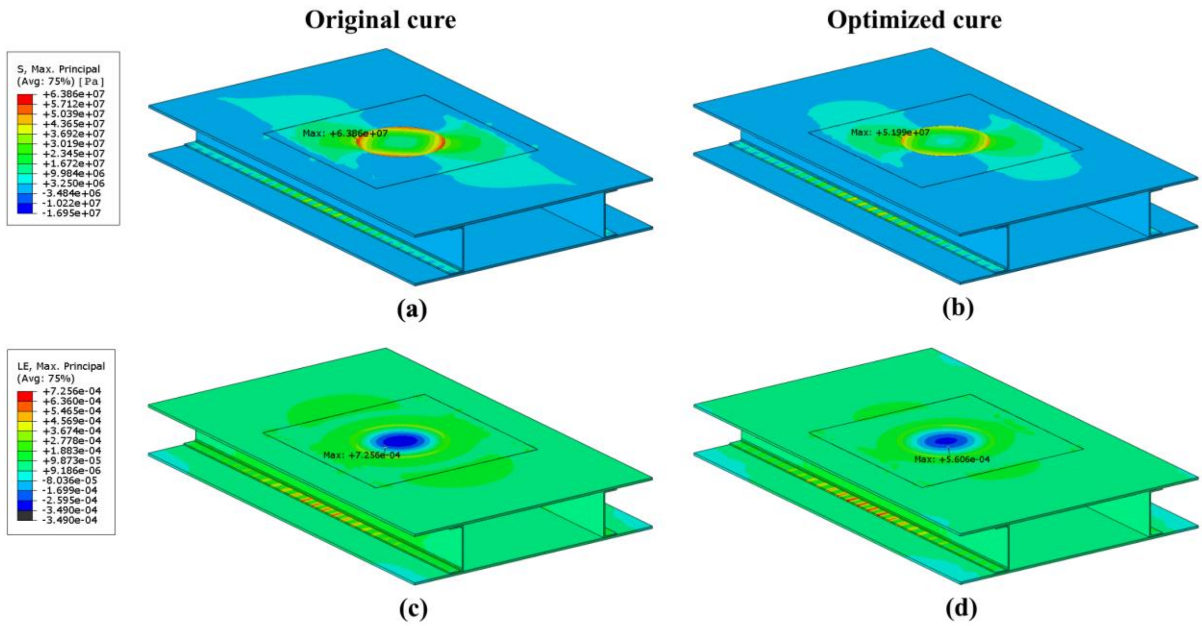

Figure 8: Results of the cure simulation on the twill weave HTA40 RM3000 scarf repair in the CYCOM-5250-4 skin of a generic wing box with (a and c) the original cure cycle and (b and d) the optimized cure cycle. (a) and (b) show the residual max principal stress and (c) and (d) the logarithmic max principal strain.

6 ACKNOWLEDGEMENTS

The research presented in this paper has been performed in the scope of the Defence Technology Project “Composite infusion repair assisted by process simulation” funded by the Dutch Ministry of Defence, Defence order number *4501255425 NTP 17-21*. The authors are grateful to John Bronder of the Dutch Ministry of Defence for the contributions and feedback to the research described in this paper.

REFERENCES

[1] A. A. Johnston, An integrated model of the development of process-induced deformation in autoclave processing of composite structures, Vanvouver: The University of British Columbia, 1997.

[2] S. Wijskamp, Shape distortions in composites forming, Enschede: Universiteit Twente, 2005.

[3] T. Garstka, Separation of process induced distortions in curved composite laminates, Bristol: University of Bristol, 2005.

[4] J. M. Svanberg, Predictions of Manufacturing Induced Shape Distortions, Luleå: Luleå University of Technology, 2002.

[5] M. W. Nielsen, Prediction of process induced shape distortions and residual stresses in large fibre reinforced composite laminates, Copenhagen: Technical University of Denmark, 2012.

[6] K. VanClooster, J. Gilbert, F. Pascon and L. V. Stepan, “Predicting the Influence of Manufacturing Parameters on Curing Generated Deformations Using Thermo-mechanical Modelling,” in *American Society for Composites*, Seattle, 2018.

[7] V. Chabridon, “Robust Probabilistic Analyses of Composite Part Manufacturing,” National Aerospace Laboratory NLR, Amsterdam, 2014.

[8] M. Ridha, V. B. Tan and T. E. Tay, “Traction-separation laws for progressive failure of bonded scar repair of composite panel,” *Composite structures,* vol. 93, no. 4, pp. 1239-1245, 2011.

[9] P. G. Slattery, C. T. McCarthy and R. M. O'Higgings, “Assessment of residual strength of repaired solid laminate composite materials through mechanical testing,” *Composite Structures,* vol. 147, pp. 122-130, 2016.

[10] M. Hautier, D. Lévêque, C. Huchette and P. Olivier, “Investigation of composite repair method by liquid resin infiltration,” *Plastics, Rubber and Composites,* vol. 39, no. 3-5, pp. 200-207, 2010.

[11] A. Kondratiev, V. Pistek, L. Smovziuk, M. Shevtsova, A. Fomina, P. Kučera and A. Prokop, “Effects of the Temperature-Time Regime of Curing of Composite Patch on Repair Process Efficiency,” *Polymers,* vol. 13, p. 4342, 2021.

[12] T. Koenis, N. v. Hoorn and W. v. d. Brink, “Calibration and Validation of a Numerical Curing Model Using AS4/8552 Asymmetric Laminated Composite Plates,” in *Presentations to VIII Conference on Mechanical Response of Composites*, Gothenburg, 2021.

[13] M. R. Kamal and S. Sourour, “Kinetics and thermal characterization of thermoset cure,” *Polym Eng Sci,* vol. 13, pp. 59-64, 1973.

[14] G. Struzziero, B. Remy and A. A. Skordos, “Measurement of thermal conductivity of epoxy resins during cure,” *Journal of Applied Polymer science,* vol. 136, p. 47015, 2019.

[15] N. Pantelelis, E. Bistekos, W. Gerrits, S. Wilkens, D. Breen and S. Wilson, “Non-intrusive intelligent cure monitoring for enhancing the manufacturing of high-temp composite structures,” in *SAMPE Europe Conference 2021*, Baden/Zürich, 2021.

[16] J. Gao, L. Li, Y. Deng, Z. Gao, C. Xu and Z. Mingxi, “Study of gelation using Differential Scanning Calorimetry (DSC),” *Journal of Thermal Analysis,* vol. 49, pp. 303-310, 1997.

[17] N. Zobeiry and A. Poursartip, “The origins of residual stress and its evaluation in composite materials,” *Structural Interity and Durability of Advanced Composites,* pp. 43-72, 2015.

[18] C. C. Chamis, *NASA Tech. Memo 8329,* 1983.

[19] C. C. Chamis, F. Abdi, M. Garg, L. Minnetyan, H. Baid, D. Huang, J. Housner and F. Talagani, “Micromechanics-based progressive failure analysis prediction for WWFE-III composite coupon test cases,” *Journal of Composite Materials,* vol. 47, no. 20, pp. 2695-2712, 2013.

[20] N. van Hoorn, C. Kassapoglou and W. M. van den Brink, “Impact repsonse prediction and sensitivity analysis of thick laminated composite plates,” Royal NLR, Amsterdam, 2020.

[21] T. Ishikawa and T.-W. Chou, “In-Plane Thermal Expansion and Thermal Bending Coefficients of Fabric Composites,” *Journal of Composite Materials,* vol. 17, no. 2, pp. 92-104, 1983.

[22] A. Saltelli, P. Annoni, I. Azzini, F. Campolongo, M. Ratto and S. Tarantola, “Variance based sensitivity analysis of model output. Design and estimato for the total sensitivity index,” *Computer Physics Communications,* vol. 181, no. 2, pp. 259-270, 2010.

[23] I. M. Sobol, “Global sensitivity indices for nonlinear mathematical models and their Monte Carlo estimates,” *Mathematics and Computers in Simulation,* vol. 55, no. 1-3, pp. 271-280, 2001.

[24] C. E. Materials, *Cycom 5250-4 Prepreg System Technical Data Sheet,* 2011.

[25] L. Moser, Experimental Analysis and Modeling of Susceptorless Induction Welding of High Performance Thermoplastic Polymer Composites, Kaiserslautern: Technische Universität Kaiserslautern, 2012.